Supplementary Figures

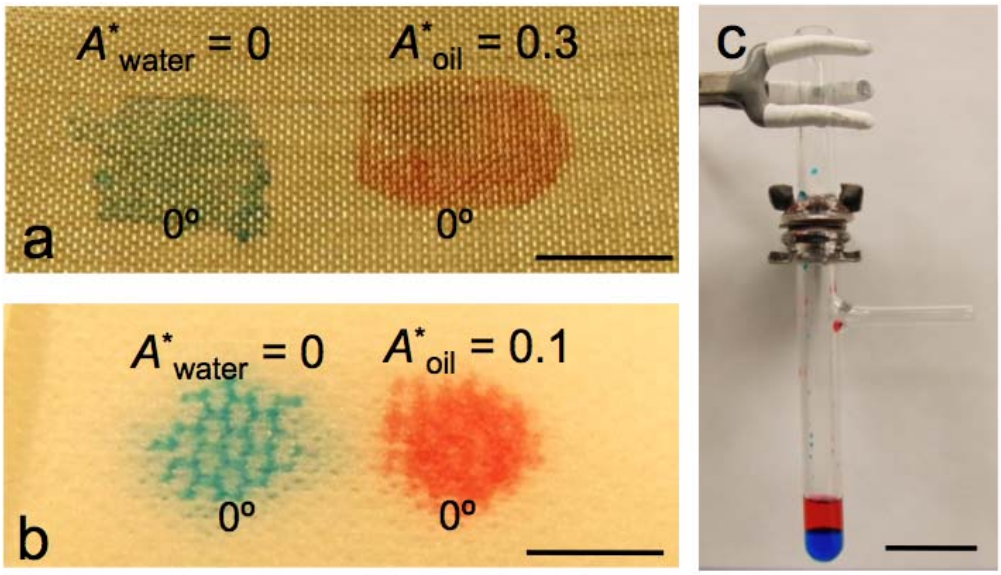

Supplementary Figure S1. Hydrophilic and oleophilic membranes. a, and **b**, Neat x-PEGDA dip-coated mesh 100 and polyester fabric membranes, respectively. Both water (dyed blue) and rapeseed oil (dyed red) readily permeate through these membranes. Scale bars, 5 mm. **c**, A mesh 100 ($2D$ = 138 μm) coated with neat x-PEGDA sandwiched between two vertical glass tubes. Both water and rapeseed oil readily permeate through the membrane. Scale bar, 2 cm.

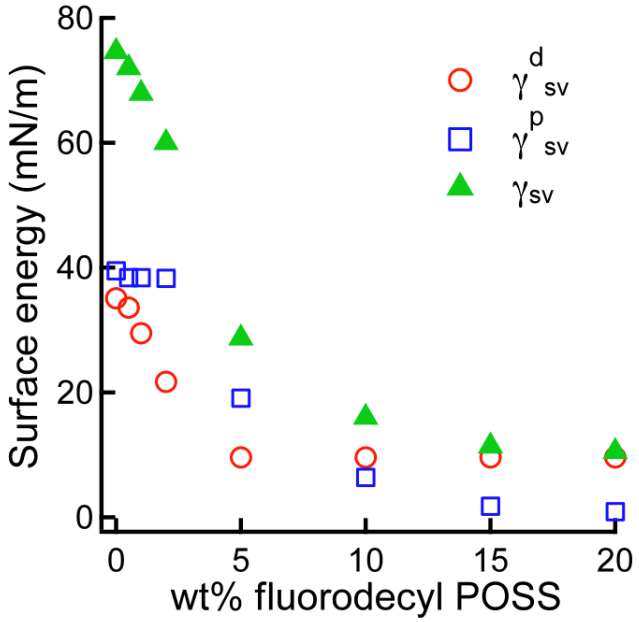

Supplementary Figure S2. Solid surface energy. The polar component (γ^{p}_{sv}), the dispersive component (γ^{d}_{sv}) and total surface energy (γ_{sv}) values for the as-prepared fluorodecyl POSS + x-PEGDA blends.

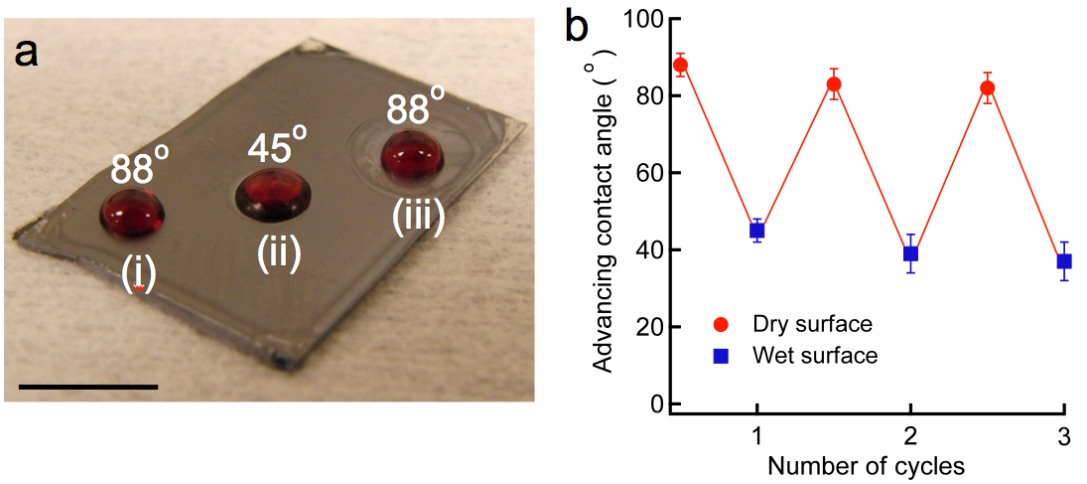

Supplementary Figure S3. Reversible stimuli-responsive surface. a, Rapeseed oil (i) at a dry location, (ii) at a location previously wet by water, (iii) at a location that was wet by water and subsequently dried. Scale bar, 1 cm. **b**, Contact angle of rapeseed oil as a function of water wetting-drying cycles.

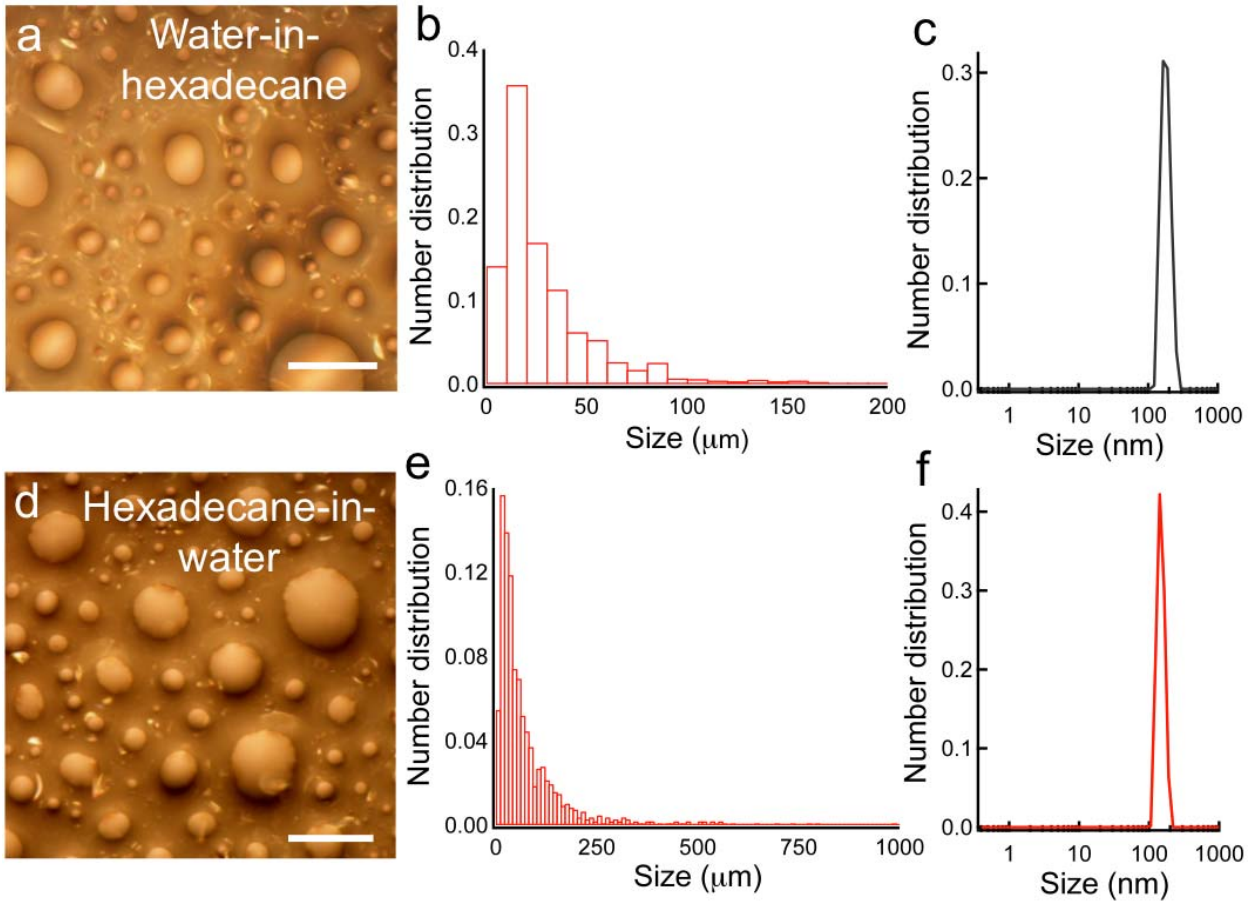

Supplementary Figure S4. Size distribution of dispersed phase in feed emulsions. a, A representative optical microscopy image of the 30:70 v:v water-in-hexadecane feed emulsion. Scale bar, 200 μm. **b**, and **c**, The number size distributions for the water-in-hexadecane feed emulsion for droplets > 1 μm and < 1 μm, respectively. **d**, A representative optical microscopy image of the 50:50 v:v hexadecane-in-water feed emulsion. Scale bar, 500 μm. **e**, and **f**, The number size distributions for the hexadecane-in-water feed emulsion for droplets > 1 μm and < 1 μm, respectively.

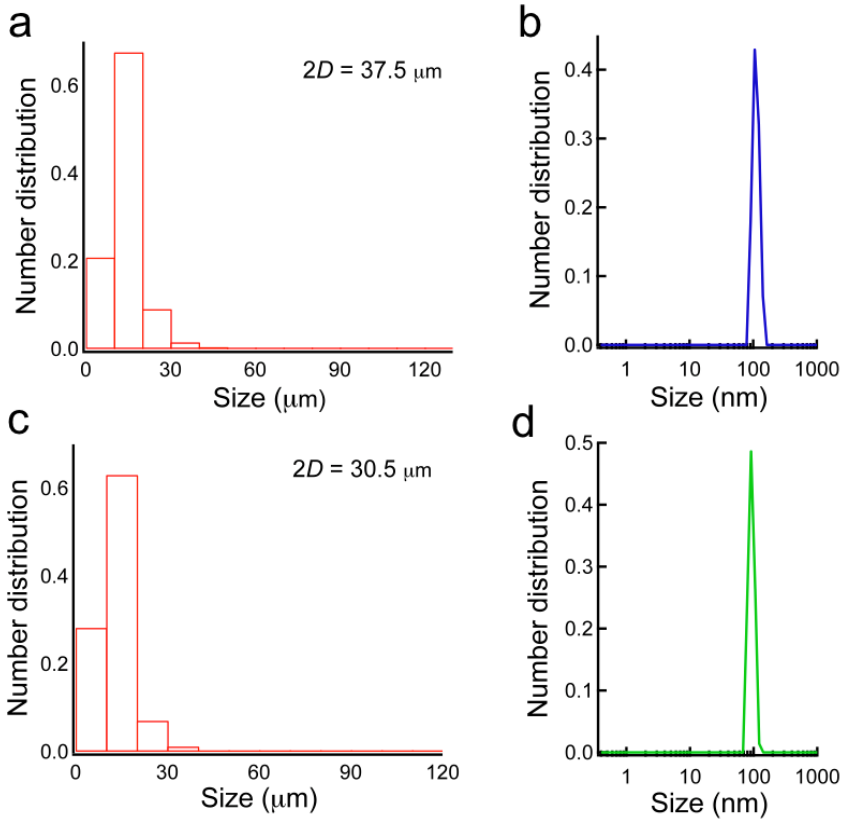

Supplementary Figure S5. Size distribution of dispersed phase in permeates. a, and **b,** The number size distributions of the permeate from the separation of the 50:50 v:v hexadecane-in-water emulsion using mesh 400, obtained with optical image analysis and DLS, respectively. **c,** and **d,** The number size distributions of the permeate from the separation of the 50:50 v:v hexadecane-in-water emulsion using mesh 500, obtained with optical image analysis and DLS, respectively.

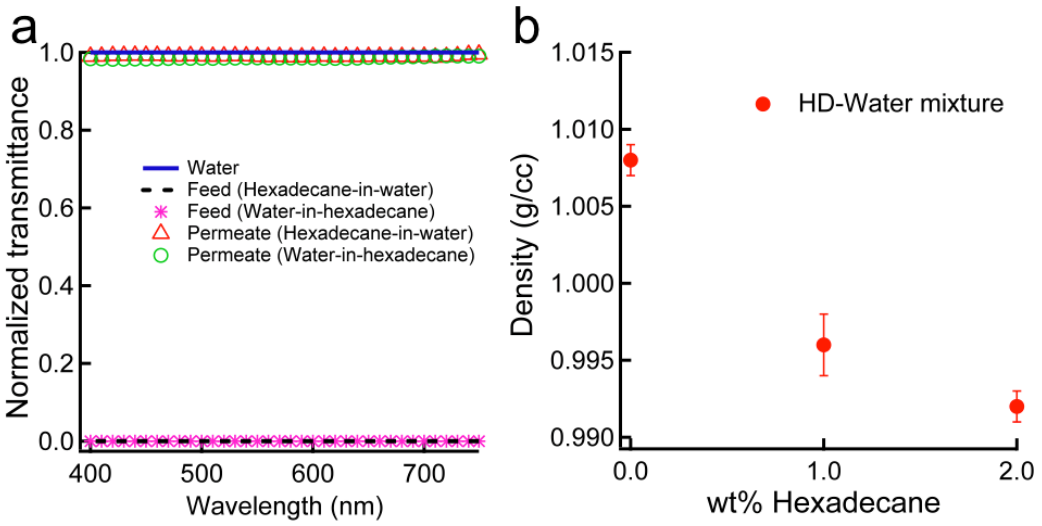

Supplementary Figure S6. Transmittance and density measurements. a, Transmittance of 50:50 v:v hexadecane-in-water, 30:70 v:v water-in-hexadecane feed emulsions and the corresponding permeates. **b,** Density of hexadecane-water mixtures as a function of hexadecane (HD) composition.

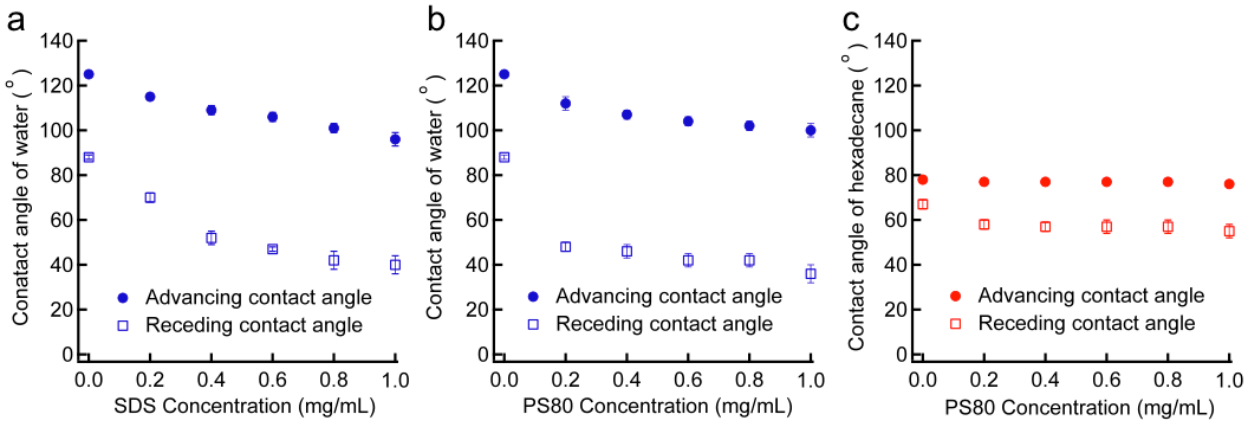

Supplementary Figure S7. Location and concentration of surfactant after emulsion separation. a, and **b,** Advancing and receding contact angles of water as a function of SDS concentration and PS80 concentration, respectively. **c,** Advancing and receding contact angles of hexadecane as a function of PS80 concentration.

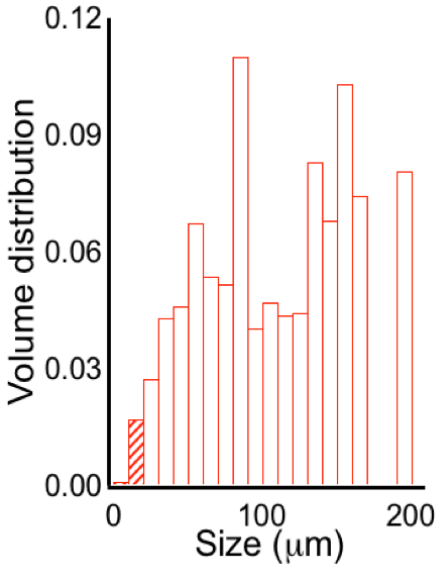

Supplementary Figure S8. Volume size distribution. Volume size distribution of water droplets for the 30:70 v:v water-in-hexadecane feed emulsion. The dashed region represents droplets below 20 μm (emulsified droplets).

Supplementary Tables

Supplementary Table S1. Contact angles and surface energies for the materials used.

Solid surface	$\theta_{oil,\,adv}$	$\theta_{oil,\,rec}$	$\theta_{water,\,adv}$	$\theta_{water,\,rec}$	γ^{d}_{sv} (mN m^{-1})	γ^{p}_{sv} (mN m^{-1})	γ_{sv} (mN m^{-1})
x-PEGDA	10º	0º	0º	0º	35.2	39.5	74.7
0.5 wt% fluorodecyl POSS + x-PEGDA	20º	0º	15º*	0º	33.6	38.4	72.0
1 wt% fluorodecyl POSS + x-PEGDA	35º	0º	23º*	0º	29.5	38.4	67.9
2 wt% fluorodecyl POSS + x-PEGDA	56º	0º	35º*	0º	21.7	38.3	60.0
5 wt% fluorodecyl POSS + x-PEGDA	88º	76º	75º*	0º	9.6	19.1	28.7
10 wt% fluorodecyl POSS + x-PEGDA	88º	82º	96º*	0º	9.6	6.4	16.0
15 wt% fluorodecyl POSS + x-PEGDA	88º	81º	110º*	0º	9.6	1.8	11.4
20 wt% fluorodecyl POSS + x-PEGDA	88º	85º	115º*	0º	9.6	0.9	10.5
Desmopan	20º	10º	89º	52º	33.6	2.0	35.6
50 wt% fluorodecyl POSS + Tecnoflon	88º	78º	120º	100º	9.6	0.3	9.9

*This is the advancing contact angle of water when water first contacts the reconfigurable surfaces. After a short duration (the time of wetting), the contact angle on these surfaces reduces to 0º.

Supplementary Table S2. Measured fluxes for the water-rich permeate and the hexadecane-rich permeate during the continuous separation of 30:70 v:v water-in-hexadecane emulsions as a function of time.

Time (h)	Water-rich permeate flux ($l\ m^{-2}\ h^{-1}$)	Hexadecane-rich permeate flux ($l\ m^{-2}\ h^{-1}$)	Time (h)	Water-rich permeate flux ($l\ m^{-2}\ h^{-1}$)	Hexadecane-rich permeate flux ($l\ m^{-2}\ h^{-1}$)
0	91.7	213.9	52	91.7	210.8
4	94.7	213.9	56	94.7	210.8
8	91.7	210.8	60	91.7	213.9
12	88.6	213.9	64	88.6	213.9
16	88.6	217.0	68	88.6	217.0
20	91.7	217.0	72	91.7	217.0
24	88.6	213.9	76	88.6	213.9
28	91.7	217.0	80	91.7	217.0
32	94.7	213.9	84	94.7	213.9
36	91.7	210.8	88	94.7	210.8
40	91.7	217.0	92	88.6	217.0
44	94.7	213.9	96	88.6	210.8
48	91.7	207.8	100	91.7	213.9

Supplementary Discussion

Free oil and water are inseparable using a hydrophilic and oleophilic membrane.

Based on previous literature[15,41], we consider surfaces with water contact angles > 150°, > 90°, < 90° and 0° as superhydrophobic, hydrophobic, hydrophilic and superhydrophilic respectively. In this case, the medium surrounding the water droplet may be either oil or air. Similarly, surfaces with oil contact angles > 150°, > 90°, < 90° and 0° are considered superoleophobic, oleophobic, oleophilic and superoleophilic respectively. In this case, the medium surrounding oil may be either water or air.

Superhydrophilic and superoleophilic membranes, such as those coated with neat x-PEGDA, cannot be used for the separation of water-in-oil emulsions or for the separation of free oil and water because both oil and water will easily permeate through the membrane (see Supplementary Figs. S1a and S1b), unless every pore within the membrane is pre-wet by water. Further, oil easily permeates through the membrane if water dries out from even a single pore within the hydrophilic membrane, which can typically happen in a matter of minutes. Supplementary Fig. S1c shows a neat x-PEGDA coated mesh 100 sandwiched between two vertical glass tubes. As soon as free rapeseed oil and water are added to the upper tube, they permeate through the membrane and are collected in the lower tube. In contrast, the superhydrophilic and oleophobic (or superoleophobic) membranes developed in this work allow for the separation of oil-in-water emulsions, water-in-oil emulsions and free oil and water (see main manuscript) without any pre-wetting. Further, these membranes prevent the permeation of oil even after water completely dries from the pores.

Estimation of the solid surface energy.

We used the Owens and Wendt approach[42] to estimate the surface energy γ_{sv} of the fluorodecyl POSS + x-PEGDA blends (Supplementary Fig. S2) and other surfaces used in this work. We used rapeseed oil (γ_{lv} = 35.7 mN m^{-1}) as the non-polar liquid to estimate the dispersive component of the solid surface energy γ^{d}_{sv} and water (γ^{d}_{lv} = 21.1 mN m^{-1} and γ^{p}_{lv} = 51.0 mN m^{-1}) as the polar liquid to estimate the polar component of the solid surface energy γ^{p}_{sv}. Supplementary Table S1 summarizes the solid surface energy values estimated by using spin-

coated flat substrates. Note that for all surfaces containing x-PEGDA, the contact angles of water reported in Supplementary Table S1 are the instantaneous values observed when water first contacts the solid surface. These values were used to estimate γ^{p}_{sv}. As mentioned in the main manuscript (see Fig. 2d in the main manuscript), due to surface reconfiguration, water contact angle decreases to 0° within a short period of time (time of wetting) on fluorodecyl POSS + x-PEGDA coated surfaces. As a result, for all fluorodecyl POSS + x-PEGDA blends, both γ^{p}_{sv} and γ_{sv} change with time.

Contact angle of rapeseed oil on a reversible stimuli-responsive surface.

Supplementary Fig. S3a shows three drops of rapeseed oil (dyed red) on a substrate spin-coated with a 20 wt% fluorodecyl POSS + x-PEGDA blend. At a dry location (i), rapeseed oil shows an advancing contact angle of $\theta_{oil,adv}$ = 88° because the majority of the surface is covered with fluorodecyl POSS domains (see main manuscript). At a location wet by water (ii), the advancing contact angle of rapeseed oil is significantly lower ($\theta_{oil,adv}$ = 45°), indicating that the surface has reconfigured to expose PEGDA chains (see main manuscript, and Supplementary Movie 1). At a location that was previously wet by water and subsequently dried completely (iii), rapeseed oil shows an advancing contact angle of $\theta_{oil,adv}$ = 88°, indicating that the surface has reverted back to its original configuration, i.e., fluorodecyl POSS domains cover the majority of the surface. This reversible stimuli-responsive surface reconfiguration is similar to the so-called "flip-flop" mechanism discussed in previous reports[21]. We conducted multiple water wetting-drying cycles and found the rapeseed oil contact angle at a fixed location to cycle between $\theta_{oil,adv}$ ≈ 88º (dry) and $\theta_{oil,adv}$ ≈ 45º, as shown in Supplementary Fig. S3b.

Surface energy analysis to estimate the degree of surface reconfiguration.

We can theoretically estimate the degree of surface reconfiguration, i.e., the relative amounts of x-PEGDA and fluorodecyl POSS in a solid surface previously wet by water. For a spin-coated surface of 20 wt% fluorodecyl POSS + x-PEGDA previously wet by water, using the Owens and Wendt approach[42] and noting that rapeseed oil shows an advancing contact angle of $\theta_{oil,adv}$ = 45º (Supplementary Fig. S3a), we obtain the dispersive component of surface energy γ^{d}_{sv}

= 26 mN m^{-1} and the polar component of surface energy γ^p_{sv} = 46.5 mN m^{-1}. Thus, the solid surface energy $\gamma_{sv} = \gamma^d_{sv} + \gamma^p_{sv}$ = 72.5 mN m^{-1}.

If the surface were assumed to be completely dry (no water), an advancing contact angle $\theta_{oil,adv}$ = 45º corresponds to a surface with ~ 1.5 wt% fluorodecyl POSS + x-PEGDA blend (see Supplementary Table S1). However, a completely dry surface is unlikely immediately after surface reconfiguration. This is evident from a higher value of γ^p_{sv} = 46.5 mN m^{-1} for the reconfigured surface, compared to γ^p_{sv} = 39.5 mN m^{-1} for neat x-PEGDA. On the other hand, if the surface were assumed to be completely wet by water, γ_{sv} = 72.5 mN m^{-1} corresponds to a surface with ~ 0.4 wt% fluorodecyl POSS + x-PEGDA blend (see Supplementary Table S1). Based on this analysis, we estimate that after reconfiguration, the surface is equivalent to an x-PEGDA blend with ~ 0.4–1.5 wt% fluorodecyl POSS.

Size distribution of the dispersed phase in the feed emulsions and permeates.

We determined the size distributions of the dispersed phase in feed emulsions and permeates using two techniques – optical microscopy image analysis for droplets above 1 μm in diameter and dynamic light scattering (DLS) for droplets below 1 μm in diameter. Supplementary Figs. S4a and S4d show representative optical microscopy images of the 30:70 v:v water-in-hexadecane and 50:50 v:v hexadecane-in-water feed emulsions, respectively. Supplementary Figs. S4b and S4e show the number size distributions of the dispersed phase, determined using image analysis. Supplementary Figs. S4c and S4f show the number size distributions of the dispersed phase, determined using DLS. The size of dispersed phase in both the feed emulsions shows a distribution with average sizes between 100–200 nm and 10–20 μm.

Supplementary Figs. S5a and S5c show the number size distribution of the permeates obtained from the separation of 50:50 v:v hexadecane-in-water emulsion using mesh 400 ($2D$ = 37.5 μm) and mesh 500 ($2D$ = 30.5 μm), respectively. These were determined using image analysis. The average size of the dispersed phase in both permeates is between 10–20 μm.
Comparing hexadecane-in-water feed emulsion with the permeates, it is evident that nearly all hexadecane droplets above 40 μm were removed during separation.

Supplementary Figs. S5b and S5d show the number size distribution of the permeates obtained from the separation of the 50:50 v:v hexadecane-in-water emulsion using mesh 400 and

mesh 500, respectively. These were determined using DLS. The average size of dispersed phase in both the permeates is approximately 100 nm. Comparing the hexadecane-in-water feed emulsion with the permeates, it is evident that the droplet size distribution below 1 μm remains almost unchanged during separation.

Methods to estimate separation efficiency.

In addition to using thermogravimetric analysis, we used the following three techniques to estimate the separation efficiency of our capillary force-based separation (CFS) processes:

A. Transmittance measurements.

We conducted transmittance measurements in order to estimate the permeate (water-rich phase) quality in batch separation relative to the feed emulsions. Supplementary Fig. S6a shows the transmittance of 50:50 v:v hexadecane-in-water and 30:70 v:v water-in-hexadecane feed emulsions (absorbance normalized to 1), transmittance of the corresponding permeates, and transmittance of pure water between 390 nm and 750 nm (visible spectrum). It is evident that both the feed emulsions are very turbid, while the corresponding permeates are very clear. This indicates that CFS used here leads to nearly complete separation.

B. Density measurements.

We also estimated the degree of separation obtained using our batch CFS by comparing the density of the permeates with density calibration curves (Supplementary Fig. S6b). We developed the calibration curves by measuring the densities of hexadecane-water mixtures with different hexadecane compositions (0 wt%, 1 wt% and 2 wt%). We measured the density of the permeates from separation of the 50:50 v:v hexadecane-in-water and 30:70 v:v water-in-hexadecane emulsions to be 1.004±0.003 g cm^{-3} and 1.006±0.004 g cm^{-3}, respectively. Comparing them with the calibration curves indicates that the permeates have significantly < 1 wt% hexadecane, confirming the separation efficiency for the CFS processes to be > 99%.

C. Karl Fischer analysis.

Karl Fischer analysis is widely used to estimate water content in various oils[43]. The retentates from the batch separation of 30:70 v:v water-in-hexadecane and 50:50 v:v hexadecane-in-water emulsions were determined to contain ~ 0.6 wt% water each. The hexadecane-rich permeate from the continuous separation of 30:70 v:v water-in-hexadecane emulsion was determined to contain ~ 25±8 ppm water (i.e., ~ 0.0025 wt% water). Note that the as-obtained

hexadecane contains ~ 20±5 ppm water. Further, the solubility of water in hexadecane at room temperature is between ~ 20-50 ppm[44,45]. This indicates that we are removing nearly all of the surfactant-stabilized (or emulsified) water droplets during the separation.

Estimation of hexadecane-water interfacial tension in the presence of surfactants.

We estimated hexadecane-water interfacial tension γ_{ow} in the presence of surfactants by using the relationship postulated by Fowkes[38]:

$$\gamma_{ow} = \gamma_{ov} + \gamma_{wv} - 2\sqrt{\gamma^{d}_{ov}\gamma^{d}_{wv}} \qquad \text{(S1)}$$

Note that here we use γ_{ow} to refer to hexadecane-water interfacial tension instead of γ_{12}, as used in the main manuscript. γ_{ov} and γ_{wv} are the surface tensions, while γ^{d}_{ov} and γ^{d}_{wv} are the dispersive components of the surface tensions of hexadecane and water, respectively, in the presence of surfactants. Note that $\gamma_{ov} = \gamma^{d}_{ov}$ for hexadecane (non-polar liquid).

Using the capillary-rise method [37], we estimated γ_{ov} = 26.9 mN m^{-1} and γ_{wv} = 45.8 mN m^{-1} with 1 mg mL^{-1} of SDS, γ_{ov} = 24.9 mN m^{-1} with 0.2 mg mL^{-1} of PS80 and γ_{wv} = 45.1 mN m^{-1} with 0.8 mg mL^{-1} of PS80.

In order to estimate γ^{d}_{wv}, we combined the Young's equation[20] with the relationship postulated by Fowkes[38] for the interfacial tension of a non-polar solid (such as a 50 wt% fluorodecyl POSS + Tecnoflon blend[28]) and water to obtain:

$$\gamma^{d}_{wv} = \frac{\left[\gamma_{wv}\left(1+\cos\theta\right)\right]}{4\gamma^{d}_{sv}} \qquad \text{(S2)}$$

Here, γ^{d}_{sv} is the dispersive component of the solid surface energy and θ is the Young's contact angle for water. The 50 wt% fluorodecyl POSS + Tecnoflon blend (γ^{d}_{sv} = 9.6 mN m^{-1}; see Supplementary Table S1) was chosen because it is essentially non-polar[28] and does not reconfigure when in contact with water or hexadecane. On a spin-coated surface of 50 wt% fluorodecyl POSS + Tecnoflon, we measured the advancing contact angles of water $\theta_{water,adv}$ = 94° and $\theta_{water,adv}$ = 95° with 1mg mL^{-1} of SDS and 0.8 mg mL^{-1} of PS80, respectively. Using these values and the previously estimated values of γ_{wv} in equation (S2), we determined γ^{d}_{wv} = 43.8 mN m^{-1} and γ^{d}_{wv} = 44.1 mN m^{-1} with SDS and PS80, respectively.

Using the values estimated above in equation (S1), we determined γ_{ow} = 4.0 mN m^{-1} with SDS and γ_{ow} = 3.7 mN m^{-1} and with PS80. As may be expected, these values are significantly

lower than the hexadecane-water interfacial tension (γ_{ow} = 51.4 mN m^{-1}) in the absence of surfactants. These estimated values of γ_{ow} were used to calculate the breakthrough height $h_{breakthrough}$ (see main manuscript) of hexadecane for 50:50 v:v hexadecane-in-water and 30:70 v:v water-in-hexadecane emulsions. The predicted values were 2.3 cm and 2.4 cm, respectively. These values closely match experimentally measured values of 2 cm and 2.2 cm, respectively.

Location and concentration of surfactant after emulsion separation.

We estimate the amount of surfactant in the permeates after emulsion separation by measuring the permeate contact angles and comparing them with calibration curves of contact angles of water and hexadecane as a function of surfactant concentration. The calibration curves were developed by measuring the contact angles on flat surfaces spin-coated with a 50 wt% fluorodecyl POSS + Tecnoflon blend. The 50 wt% fluorodecyl POSS + Tecnoflon blend was chosen because it is essentially non-polar (see Supplementary Table S1) and it does not reconfigure when in contact with either water or hexadecane. Supplementary Figs. S7a and S7b show the advancing and receding contact angles of water as a function of SDS and PS80 concentration. Supplementary Fig. S7c shows the advancing and receding contact angles of hexadecane as a function of PS80 concentration. As SDS is nearly insoluble in hexadecane, we could not obtain the corresponding calibration curve.

Consider the permeate (~ 99.9 wt% water) from batch separation of SDS stabilized 50:50 v:v hexadecane-in-water emulsion. The advancing and receding contact angles of the permeate are 94°±2° and 39°±4°. By comparing these contact angles with Supplementary Fig. S7a, it is evident that the concentration of SDS in the permeate is approximately 1 mg mL^{-1}. In other words, after separation, nearly all the surfactant is in the permeate. This is likely due to the fact that SDS is nearly insoluble in hexadecane. Similarly, since span80 in nearly insoluble in water, we found that after separation of span80 stabilized water-in-hexadecane emulsions, nearly all the surfactant is in the retentate.

Now consider the two permeates from continuous separation of PS80 stabilized 30:70 v:v water-in-hexadecane emulsion. The advancing and receding contact angles of the water-rich permeate (~ 99.9 wt% water) through the superhydrophilic and oleophobic membrane are 98°±2° and 38°±4°, while those of the hexadecane-rich permeate (~ 99.9 wt% hexadecane) through the hydrophobic and oleophilic membrane are 76°±2° and 56°±4°. By comparing these contact

angles with Supplementary Fig. S7b and S7c, it is evident that the concentration of PS80 in the water-rich permeate is between 0.8–1 mg mL^{-1}, while the concentration of PS80 in the hexadecane-rich permeate is between 0–0.2 mg mL^{-1}. This is because of the higher solubility of PS80 in water when compared to hexadecane.

Fraction of emulsified water droplets removed from water-in-hexadecane feed emulsions during continuous separation.

100 mL of 30:70 v:v water-in-hexadecane feed emulsion contains 30 mL of water and 70 mL of hexadecane. We determined the volume fraction of emulsified water droplets (< 20 μm) in our feed emulsions to be 0.018 from the volume size distribution (see Supplementary Fig. S8). Thus, the volume of emulsified water droplets in 100 mL of feed emulsion is 0.54 mL. In continuous separation, 100 mL of feed emulsion results in approximately 30 mL of water-rich permeate and 70 mL of hexadecane-rich permeate. Karl Fischer analysis indicates that the amount of water in the hexadecane-rich permeate is ~ 0.0025 wt%, which is equivalent to ~ 0.0019 vol%. Thus, the volume of water in the hexadecane-rich permeate is 0.0013 mL. Even if we assume that the size of all the water droplets in the hexadecane-rich permeate is < 20 μm, comparing the volume of the emulsified water droplets in the feed emulsion (0.54 mL) to that in the hexadecane-rich permeate (0.0013 mL), we conclude that the volumetric fraction of emulsified droplets removed during separation is at least 99.8%.

Prediction of water-rich permeate and hexadecane-rich permeate fluxes during the continuous separation of water-in-hexadecane emulsions.

We seek to predict the flux of water-rich permeate through the superhydrophilic and oleophobic mesh 400 and the flux of hexadecane-rich permeate through the hydrophobic and oleophilic mesh 400 used in the continuous separation of 30:70 v:v water-in-hexadecane emulsions. In this analysis, we assume that the water-rich permeate (≤ 0.1 wt% hexadecane) and the hexadecane-rich permeate (≤ 0.1 wt% water) have the same fluid flow characteristics as those of pure water and pure hexadecane, respectively.

Consider the flow of water-rich permeate through the superhydrophilic and oleophobic membrane. For a 30:70 v:v water-in-hexadecane emulsion column of height 1.2 cm above mesh 400 (R = 12.5 μm, $2D$ = 37.5 μm), the flux of water-rich permeate (μ = 1 mPa-s) predicted using the Hagen-Poiseuille relation[37] is 88,400 l m^{-2} h^{-1}. This is three orders of magnitude higher than

the experimentally measured flux of 90 l m^{-2} h^{-1} (see Fig. 5c in the main manuscript, Supplementary Table S2). Such a large discrepancy arises from the assumption that the water droplets (dispersed phase) are constantly in contact with the membrane, so that they may readily permeate through, without any discontinuity. In reality, a majority of the dispersed water droplets are not in physical contact with the membrane. Each dispersed water droplet must settle (or sediment) under gravity, reach the membrane, wet the membrane and permeate through. The rate of sedimentation decreases rapidly as the size of the dispersed water droplets decreases. Consequently, the flux for the water-rich permeate is limited by the rate of sedimentation of water droplets. Ishii and Zuber[46] conducted a comprehensive analysis on the sedimentation velocity v_d of droplets in dispersions to arrive at equations (S3)-(S6) and validated them through extensive sets of experiments. They suggest:

$$v_{\mathrm{d}} = v_{\mathrm{r}}\left(1-\alpha_{\mathrm{d}}\right) \tag{S3}$$

$$v_{\mathrm{r}}^2 = \frac{8}{3}\frac{r_{\mathrm{d}}}{C_{\mathrm{D}}\rho_{\mathrm{c}}}\left(\rho_{\mathrm{d}}-\rho_{\mathrm{c}}\right)g\left(1-\alpha_{\mathrm{d}}\right) \tag{S4}$$

$$C_{\mathrm{D}} = \frac{24}{Re} \tag{S5}$$

$$Re = \frac{2r_{\mathrm{d}}\rho_{\mathrm{c}}v_{\mathrm{r}}}{\mu_{\mathrm{m}}} \tag{S6}$$

Here, v_{r} is the relative velocity between the dispersed and the continuous phases, r_{d} is the radius of the dispersed phase droplets, C_{D} is the drag coefficient, ρ_{c} and ρ_{d} are the densities of the continuous and the dispersed phase, α_{d} is the volume fraction of the dispersed phase, and μ_{m} is the effective viscosity of the mixture. For the 30:70 v:v water-in-hexadecane emulsion used in this work, ρ_{c} = 0.77 g cm^{-3}, ρ_{d} = 1 g cm^{-3}, α_{d} = 0.3 and μ_{m} = 2.5 mPa s. We calculate the mean volumetric radius r_{d} of the water droplet as:

$$V_{\mathrm{mean}} = 4/3\,\pi r_{\mathrm{d}}^3 \tag{S7}$$

where the mean volume V_{mean} is given by:

$$V_{\mathrm{mean}} = \sum x_{\mathrm{i}}V_{\mathrm{i}} \tag{S8}$$

Here x_{i} and V_{i} refer to the number fraction and volume, respectively, of water droplets with diameter d_{i}. From the number distribution shown in Supplementary Fig. S4b, we obtain r_{d} = 28 μm. Using equations (S3)-(S6), we predict the average sedimentation velocity of water droplets

to be v_d = 77 μm s^{-1}, which leads to a water-rich permeate flux of 83 l m^{-2} h^{-1} through the superhydrophilic and oleophobic mesh 400. This value is in reasonable agreement with the experimentally measured flux of 90 l m^{-2} h^{-1}. As the sedimentation velocity is proportional to square of the droplet radius (combining equations (S3)-(S6)), the flux of water-rich permeate will be impractically low (< 1 l m^{-2} h^{-1}) for fine emulsions with droplet diameter less than 5 μm. In such cases, other techniques such as electrostatic coalescence (if the wetting phase is a polar liquid)[36], or forced convection[3], may be useful.

Now, consider the flow of hexadecane-rich permeate through the hydrophobic and oleophilic membrane. Since we conducted continuous separation at steady state with a feed flux of 300 l m^{-2} h^{-1}, material balance for a 30:70 v:v water-in-hexadecane emulsion yields a hexadecane-rich permeate flux of 217 l m^{-2} h^{-1}. This predicted flux is in reasonable agreement with the experimentally measured flux of 210 l m^{-2} h^{-1} (see Supplementary Table S2). Note that our fluxes are comparable to those reported in membrane separation literature for dead-end filtration[40] and cross-flow filtration[3], where separation was engendered using an energy intensive, externally applied pressure difference, as opposed to the sole use of gravity in this report. As the flux of hexadecane-rich permeate through the hydrophobic and oleophilic membrane is constrained by the material balance, the maximum possible flux may be significantly higher.

Supplementary References

41 Feng, X. & Jiang, L. Design and creation of superwetting/antiwetting surfaces. *Adv. Mater.* **18**, 3063-3078 (2006).

42 Owens, D. K. & Wendt, R. C. Estimation of surface free energy of polymers. *J. Appl. Polym. Sci.* **13**, 1741-1747 (1969).

43 Margolis, S. A. Amperometric measurement of moisture in transformer oil using Karl-Fischer reagents. *Anal. Chem.* **67**, 4239-4246 (1995).

44 Schatzberg, P. Solubilities of water in several normal alkanes from C7 to C16. *J. Phys. Chem.* **67**, 776-779 (1963).

45 Schatzberg.P. Diffusion of water through hydrocarbon liquids. *J. Polym. Sci. Pol. Sym*. **10**, 87-82 (1965).

46 Ishii, M. & Zuber, N. Drag coefficient and relative velocity in bubbly, droplet or particulate flows. *AICHE J.* **25**, 843-855 (1979).